2021 International Conference on Unmanned Aircraft Systems (ICUAS)
Athens, Greece. June 15-18, 2021

Forest Fire Detection and Localization Using Thermal and Visual Cameras

Mohsen Sadi, Youmin Zhang, Wen-Fang Xie, and F M Anim Hossain

Abstract— **In this paper, a system targeting for using unmanned aerial vehicle (UAV) to application of detecting and locating forest fires is developed. It utilizes the information of two cameras: one charged coupled device (CCD) camera and one thermal camera. The information of both cameras are aligned and then fused to verify if a fire has occurred. In the alignment process, a homography matrix is calculated to assure that the corresponding pixels in both images point to the same area. An image-based thermo-visual servoing (IBTVS) system is implemented for the fire tracking process. A two-degree-of-freedom (2DOF) frame is fabricated based on IBTVS to test the tracking and locating capabilities of the system. Experimental tests show that the designed system can extract fire features from thermal and visual cameras, calculate the position of fire, and command the frame for pointing to the fire.**

I. Introduction

The importance of forests in terms of balancing the nature is inevitable. They can purify water, stabilize soil and moderate climate. However, millions of hectares of forests are destroyed by fires every year. This affects almost three hundred thousand people yearly. Millions of dollars are spent to extinguish these fires [1]–[3]. These fires keep threatening the ecological systems, infrastructures, and public safety [4]. Unwanted fires can spread quickly to the areas that threaten human lives and ecological system of forests. Therefore, it is important to suppress these fires in the early stage [5].

Traditionally, to detect forest fires, these approaches are used: human patrol, ground equipment with smoke, visual and thermal sensors, manned aircraft and satellite imagery [6], [7]. These methods are not perfect and have disadvantages. For example, smoke and thermal sensors should be close to the fire and cannot give exact information on the size or location of the fire [8]. Human patrol is not reasonable in large, dense, and remote forests. Satellite images are not rich enough to detect early stage fires and they cannot continuously monitor forests [6]. Manned aerial operations are expensive. Additionally, manned operations can potentially threaten the crews' lives.

With the new developments in UAV technology, low-cost UAVs are available for research purposes. UAVs can fly over high-risk zones, yield over-the-hill view, and perform day- and night-time missions with no risk to human lives [9]. Using UAVs in forest fire detection operations has these benefits: 1) covering a wide area; 2) ability to operate for a long duration of both day- and night-time; 3) cost-effective operations 4) operating different missions based on different sensors on-board; 5) minimum disturbance to wildlife; 6) minimum operator's involvement [10].

Camera-based fire monitoring systems are categorized into visual, infrared (IR), or thermal types [8]. Fires are normally detected by their flame or smoke. To do so, it is needed to extract the features of flame or smoke. These features are mainly color, motion, and geometry [11]. Chen et al. [12] use red, green, and blue (RGB) channels as features of offline video frames to detect flame. They also make use of sequence of frames to detect smoke. In [11], the background information is removed by an adaptive subtraction system. Then a statistical color model is used to check existence of a fire. In [13], instead of RGB color space, they use YCbCr which can separate chrominance from luminance. Yuan et al. [10] present a fire detection method that makes use of the Lab color space. It separates fire pixels from non-fire pixels in channel A of this color space by using Otsu segmentation method. The performance of this method in [14] is improved by utilizing both color and motion features of a fire.

IR cameras are used in many fire detection methods [15]–[17]. In [18] and [19] the binary images are generated from IR camera information by using the threshold selection method of [20]. The false alarms are reported to be reduced significantly. In [21], the authors predict the propagation of fire by using linear transformation in IR images. Yuan et al. [22] extract fire pixels from non-fire hot objects and background pixels by using histogram-based segmentation and optical flow analysis. In order to improve fire detection algorithms, visual and IR cameras can be used together. Bosch et al. [23] fuse visual and IR camera images to detect fire. They generate some decision fusion rules to do so. Martinez de-Dios et al. [24] utilize image processing techniques and integrate both visual and IR cameras for calculating fire front parameters. The work continues in [1] and they extract a 3D fire perception from fused visual and IR images.

In this work, besides a visual camera, a thermal camera is used because thermal cameras are more sensitive to the temperature. Therefore, it is possible to detect the fire before there are huge flames. Also the detection method is improved by creating an alignment process to fuse thermal and visual images. Finally an image-based thermo-visual servoing controller is created and put on a 2DOF frame built through this work to test the functions and effectiveness of the developed system and algorithms.

This work was supported in part by Natural Sciences and Engineering Research Council of Canada. (Corresponding Author: Youmin Zhang.)

Mohsen Sadi, Youmin Zhang, Wen-Fang Xie, and F M Anim Hossain are with the Department of Mechanical, Industrial and Aerospace Engineering, Concordia University, Montreal, Quebec H3G 1M8, Canada (e-mails: mohsen.sadi@gmail.com, youmin.zhang@concordia.ca, wenfang.xie@concordia.ca, fmanim.hossain@mail.concordia.ca).

2021 International Conference on Unmanned Aircraft Systems (ICUAS) | 978-1-6654-1535-4/21/$31.00 ©2021 IEEE | DOI: 10.1109/ICUAS51884.2021.9476865

Authorized licensed use limited to: Concordia University Library. Downloaded on July 20,2021 at 14:25:49 UTC from IEEE Xplore. Restrictions apply.

The remainder of this paper is organized as: Section II describes a platform developed, and its system components and mathematical model. Section III discusses the algorithms used to detect fire and Section IV provides the test results.

II. System Components and Mathematical Model

The purpose of this research is to develop an on-board real-time forest fire monitoring system that can detect and locate any possible fire. To do so, a combination of a visual camera and a thermal camera is used. Both cameras are connected to a mini processor (Raspberry Pi 4) and all of the computations are done within the on-board Raspberry Pi. A two-degree-of-freedom (2DOF) frame is made in order to simulate and validate the fire detection and tracking capabilities of the system.

The 5-megapixels camera (OV5647 sensor) has 1080p video resolution at 30 FPS. Its field of view is $54°\times41°$. In many cases like fires covered by smokes or fires under ashes, visual cameras cannot easily detect the existence of a fire and it is the duty of thermal camera to do so. In this research, a MLX90640 thermal sensor which has a resolution of 32×24 pixels and a FOV of $55°\times35°$ is used. This is beneficial as it has a FOV close to the visual camera. In this way, it is possible to align both cameras for further usages. Fig. 1(a) shows an image of a fire taken by the visual camera and Fig. 1(b) shows the same view from the thermal camera.

(a) Visual image (b) Thermal image

Fig. 1: Visual and thermal images of a fire

A. The Model of a 2DOF Frame

A 2DOF frame is made to simulate the fire detection, localization and tracking capabilities of the system, as shown in Fig. 2. It can rotate in two directions, which is analogous to a camera mounted on a UAV, i.e. if a UAV can move in two directions (x and y, in a constant altitude z). In a UAV system, if a fire is found, its location is expressed by x and y distances while in this system the location of the fire is indicated by α_x and α_y angles. Fig. 3 illustrates the model of this system.

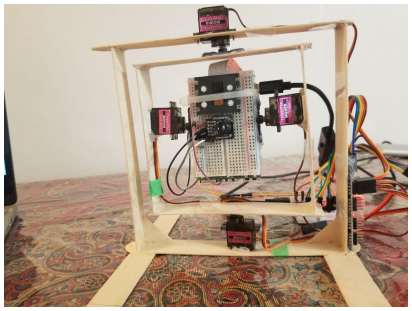

Fig. 2: 2DOF frame

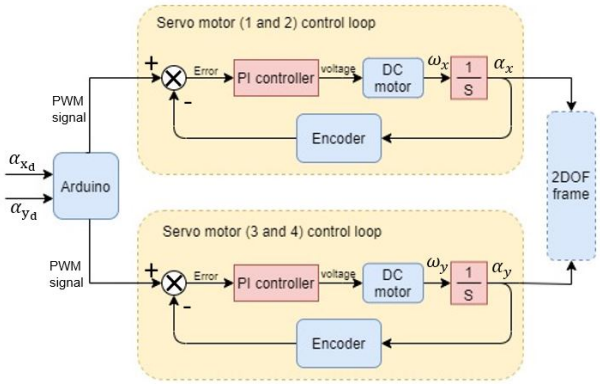

Fig. 3: The model of 2DOF frame

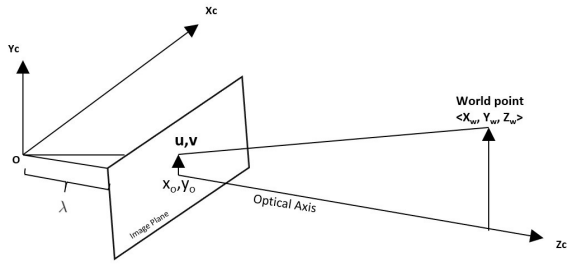

Fig. 4: Camera projection model

B. Deriving Jacobian Matrix for the 2DOF Frame

The position and velocity of any object in image can be related to the motion of camera by forming the Jacobian matrix. A point $P = [X_w, Y_w, Z_w]^T$ is in the camera coordinate system. Its projected point in the image is $f = [u, v]^T$ where u and v are pixel indices. The pose vector of camera is denoted as below:

$$r = [x_w \ y_w \ z_w \ \alpha_x \ \alpha_y \ \alpha_z]^T \tag{1}$$

where x_w, y_w, z_w are the positions in x, y, z axes w.r.t the base frame and α_x, α_y, α_z are the rotational angle around x, y, z axes. For this 2DOF frame, α_x and α_y are the inputs of this system. By differentiating (1), the velocity of camera is:

$$\dot{r} = [v_x \ v_y \ v_z \ \omega_x \ \omega_y \ \omega_z]^T \tag{2}$$

where $v_x = v_y = v_z = \omega_z = 0$, as it only rotates around x and y axes. The velocity of the projected point f is defined as:

$$\dot{f} = \begin{bmatrix} \dot{u} \\ \dot{v} \end{bmatrix} \tag{3}$$

The velocity of point P is:

$$\begin{cases} \dot{X_w} = Z_w\omega_y - Y_w\omega_z + v_x = Z_w\omega_y \\ \dot{Y_w} = X_w\omega_z - Z_w\omega_x + v_y = Z_w\omega_x \\ \dot{Z_w} = Y_w\omega_x - X_w\omega_y + v_z = Y_w\omega_x - X\omega_y \end{cases} \tag{4}$$

The relationship between P and f is given by:

$$\begin{bmatrix} u \\ v \end{bmatrix} = \frac{\lambda}{Z_w} \begin{bmatrix} X_w \\ Y_w \end{bmatrix} \tag{5}$$

where λ is the focal length of camera (λ = 3.6mm). By taking derivative from (5), one has:

$$\begin{cases} \dot{u} = \lambda \frac{Z_w\dot{X} - X_w\dot{Z}}{Z^2} \\ \dot{v} = \lambda \frac{Z_w\dot{Y} - Y_w\dot{Z}}{Z^2} \end{cases} \tag{6}$$

Authorized licensed use limited to: Concordia University Library. Downloaded on July 20,2021 at 14:25:49 UTC from IEEE Xplore. Restrictions apply.

Since u and v are image indices and start from top-left, they have to be converted to image coordinates. The origin is the center point in image coordinates. Therefore, one has

$$\begin{bmatrix} x \\ y \end{bmatrix} = \begin{bmatrix} -1 & 0 & x_0 \\ 0 & -1 & y_0 \end{bmatrix} \begin{bmatrix} u \\ v \\ 1 \end{bmatrix} \tag{7}$$

where $(x, y)^T$ is the coordinates of the point f in the image coordinates. $(x_0, y_0)^T$ is the pixel-index of center point. By putting (5) into (4), the velocity components of P are given by:

$$\begin{cases} \dot{X_w} = Z_w \omega_y \\ \dot{Y_w} = Z_w \omega_y \\ \dot{Z_w} = \frac{Z_w}{\lambda}(v\omega_x - u\omega_y) \end{cases} \tag{8}$$

Combining (6), (7) and (8), the following is derived:

$$\begin{bmatrix} \dot{x} \\ \dot{y} \end{bmatrix} = \begin{bmatrix} \frac{xy}{\lambda} & -\frac{\lambda^2+x^2}{\lambda} \\ \frac{\lambda^2+y^2}{\lambda} & -\frac{xy}{\lambda} \end{bmatrix} \begin{bmatrix} \omega_x \\ \omega_y \end{bmatrix} \tag{9}$$

Equation (9) shows a relation between the rate of rotations of camera and the velocity of a point in image coordinates. This relation is called the Jacobian matrix and is denoted by J_{image}:

$$\dot{f} = J_{image}\dot{r} \tag{10}$$

The inverse of Jacobian matrix is:

$$J_{image}^{-1} = \begin{bmatrix} \frac{\lambda xy}{D} & \frac{\lambda(\lambda^2+x^2)}{D} \\ \frac{\lambda(\lambda^2+x^2)}{D} & \frac{-\lambda xy}{D} \end{bmatrix} \tag{11}$$

where

$$D = \lambda^4 + 2\lambda^2 x^2 + x^4 + x^2 y^2$$

By combining (11) and (9), ω_x and ω_y are found in terms of speed of the point in image:

$$\begin{bmatrix} \omega_x \\ \omega_y \end{bmatrix} = J_{image}^{-1} \begin{bmatrix} \dot{x} \\ \dot{y} \end{bmatrix} \tag{12}$$

III. Fire Detection Algorithms

In this research, multiple fire detection algorithms have been proposed. The detection methods with single visual camera, single thermal camera and fusion of both cameras are implemented and compared.

A. Single Visual Camera

A pixel can be represented by three values as red, green and blue colors (RGB). For a pixel in a fire, the dominant color is red. So by putting a threshold for the red color, a fire pixel can be detected. This method can lead to a false fire detection because a white pixel will have a high value for red (as well as green and blue). Lab color space is composed of three channels: Luminance (L) and chrominances a and b. The luminance represents the level of darkness of the pixel and ranges from black (L=0) to white (L=100). Channel a is the pixel color in the spectrum of red to green and channel b is from yellow to blue. a and b have a range of -128 to 127 [10]. L, a, and b can be calculated from an RGB image as following:

$$\begin{aligned} L &= 116 \times (0.299R + 0.587G + 0.114B)^{\frac{1}{3}} - 16; \\ a &= 500 \times [1.006 \times (0.607R + 0.174G + 0.201B)^{\frac{1}{3}} \\ &\quad - (0.299R + 0.587G + 0.114B)^{\frac{1}{3}}]; \\ b &= 200 \times [(0.299R + 0.587G + 0.114B)^{\frac{1}{3}} \\ &\quad - 0.846 \times (0.066G + 1.117B)^{\frac{1}{3}}]. \end{aligned} \tag{13}$$

The advantage of using Lab color space is that unlike RGB color space, it can detect fire pixels in the images with different lighting. A fire pixel has high value of a and b in this color space since high values of a and b represent yellow and red colors. Hence, a decision-making rule can be designed. In each component (L, a or b), the average value $\bar{A}_I$ of all pixels can be computed as below [25]:

$$\bar{A}_I = \frac{1}{N} \sum_{(x,y)\in I} P_\Phi(x, y), \tag{14}$$

where $P_\Phi(x, y)$ is the value of a pixel at (x, y) position in a component of Lab color space, I is one of the components (L, a or b) and N is the total number of pixels. The decision-making rule (P_F) for fire pixel is formulated as below:

$$\begin{cases} \text{Condition 1:} & \bar{A}_L + (MAX_L - \bar{A}_L) \times 0.1 \le L \le 255; \\ \text{Condition 2:} & \bar{A}_a + (MAX_a - \bar{A}_a) \times 0.2 \le a \le 255; \\ \text{Condition 3:} & \bar{A}_b + (MAX_b - \bar{A}_b) \times 0.2 \le b \le 255; \end{cases} \tag{15}$$

where $\bar{A}_I$ is the average value of all pixels in the I^{th} component and MAX_I is the maximum amount of a pixel value in I. This decision-making rule shows acceptable result with different lighting images. Furthermore, since the final goal is to fuse visual image and thermal image, the acceptable result in this step leads to a significant result in the next step.

Fig. 5 and Fig. 6 show two fire images that use Lab fire detection algorithm. They are different in many aspects. First, they have different lighting values. Second, in the first image, there is a white smoke that can be misinterpreted as a fire. Third, in the second image, although it seems that a fire is obvious, but this image suffers from reddish background. But this method is able to detect fire pixels with a set of rules that are fixed for any condition.

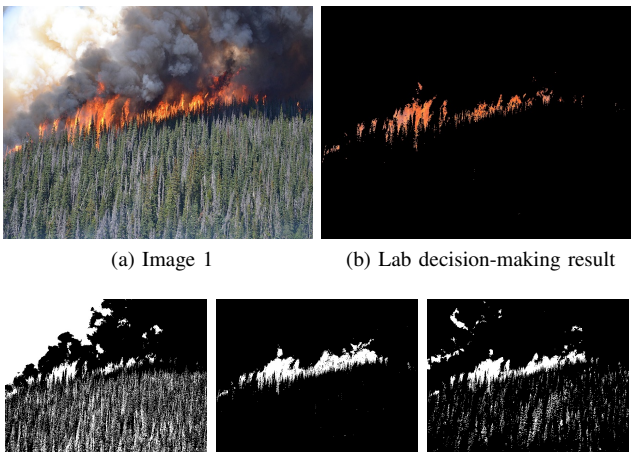

(a) Image 1 (b) Lab decision-making result

(c) Condition 1 in (15) (d) Conditions 2 in (15)(e) Conditions 3 in (15)

Fig. 5: Lab decision-making Test 1

B. Single Thermal Camera

Finding fire pixels in a thermal camera is fairly easy. Since the thermal camera has only one channel and that is the temperature of each point, by defining a threshold for fire temperature, the fire pixels can be found.

Authorized licensed use limited to: Concordia University Library. Downloaded on July 20,2021 at 14:25:49 UTC from IEEE Xplore. Restrictions apply.

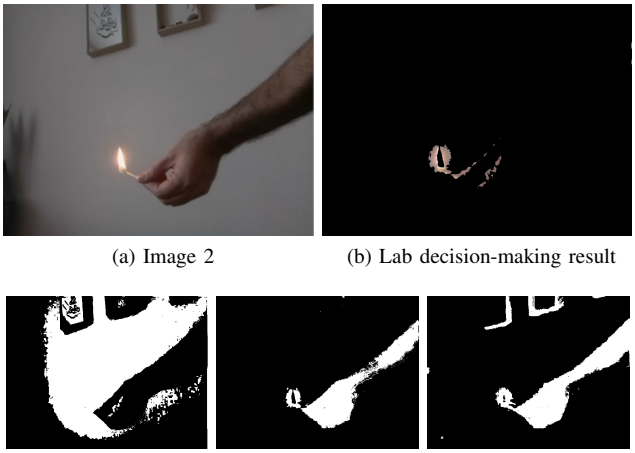

(a) Image 2 (b) Lab decision-making result

(c) Condition 1 in (15) (d) Conditions 2 in (15) (e) Conditions 3 in (15)

Fig. 6: Lab decision-making Test 2

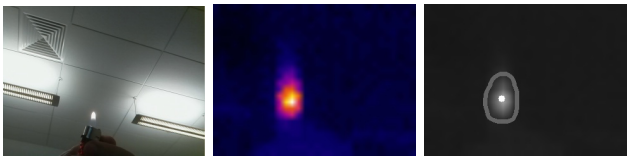

(a) Image of a flame and background light (b) Thermal image of (a) (c) Calculated fire area and its center

Fig. 7: Thermal fire detection method

C. Fusion of Visual and Thermal Images

In order to improve the precision of fire detection system, a combination of both cameras is used. First, two cameras have to be placed as close as possible to maximize the common areas. Then an alignment method should be implemented to find the corresponding pixel in each camera. Then all of the pixels are tested for fire(s). The area which is detected as fire by both cameras will be considered as a fire. Other areas that are verified only by one camera will be disregarded. Fig. 4 illustrates the camera projection model and the projective transformation of a point in (X_w, Y_w, Z_w) into the image plane pixel (u, v). Notations used in the projective transformation are listed in Table 1. The mathematical formulation is provided in the following equation.

This is called a "projective transformation". In the right hand side of the equation, the second to right matrix is called the "extrinsic parameter matrix" of the camera that transforms the world coordinate (X_w, Y_w, Z_w) into camera coordinate (X_C, Y_C, Z_C) using a rotation matrix $R_{3\times3}$ and translation matrix $t_{3\times1}$. Next, the camera coordinates are transformed into image coordinates using the leftmost matrix called the "intrinsic parameters" of the camera, that includes the focal length λ, aspect ratio a, skew of the image plane s and (x_0, y_0) is the point where the optical axis OZ_C goes through the image plane. The multiplication of the extrinsic and intrinsic parameters provides the following equation:

$$\begin{bmatrix} u \\ v \\ w \end{bmatrix} = \begin{bmatrix} m_{11} & m_{12} & m_{13} & m_{14} \\ m_{21} & m_{22} & m_{23} & m_{24} \\ m_{31} & m_{32} & m_{33} & m_{34} \end{bmatrix} \begin{bmatrix} X_w \\ Y_w \\ Z_w \\ 1 \end{bmatrix} \tag{16}$$

or in other words, $X_1^{'} = PX_1$, and where $X_1^{'}$ is the projected coordinate in homogeneous coordinate system, P is called the projective matrix and X is the point that is being projected in homogenous coordinate. In reality, the image plane is non-homogenous. The non-homogenous image points can be found by dividing the first two elements in the homogenous vector by the third one. The projection of a world point (X_w, Y_w, Z_w) into a pixel (u, v) can be computed using the following equation.

$$\begin{bmatrix} u \\ v \\ w \end{bmatrix} = \begin{bmatrix} \lambda & s & x_0 \\ 0 & a\lambda & y_0 \\ 0 & 0 & 1 \end{bmatrix} \begin{bmatrix} 1 & 0 & 0 & 0 \\ 0 & 1 & 0 & 0 \\ 0 & 0 & 1 & 0 \end{bmatrix} \begin{bmatrix} R_{3\times3} & t_{3\times1} \\ 0_{1\times3} & 1 \end{bmatrix} \begin{bmatrix} X_w \\ Y_w \\ Z_w \\ 1 \end{bmatrix} \tag{17}$$

In this project, a thermal and a visual camera are used to make the fire detection algorithm robust. The thermal camera is a 24×32 thermal array that displays the output as a grayscale image. Therefore, the sensor information fusion requires a projective transformation between two image planes. In an image plane, a point only has two dimensional values and the Z_w value in equation can be set to 0. Consequently, the third column of the projective matrix P is always multiplied with 0 and thus, it can be removed. The process of projective transformation between two planes is known as homography and follows the following equation:

$$\begin{bmatrix} x^{'} \\ y^{'} \\ w \end{bmatrix} = \begin{bmatrix} h_{11} & h_{12} & h_{13} \\ h_{21} & h_{22} & h_{23} \\ h_{31} & h_{32} & h_{33} \end{bmatrix} \begin{bmatrix} x \\ y \\ 1 \end{bmatrix} \tag{18}$$

or in other words, $X_2^{'} = HX_2$. Here, $X_2^{'}$ is the projected points in homogenous coordinate and H is called the homography matrix. The projected image coordinates can be computed as $u = x^{'}/w$ and $v = y^{'}/w$. Expanding (18) to find the non-homogenous image points, the following equations can be formed:

$$u = \frac{x^{'}}{w} = \frac{h_{11}x + h_{12}y + h_{13}}{h_{31}x + h_{32}y + h_{33}} \tag{19}$$

$$v = \frac{y^{'}}{w} = \frac{h_{21}x + h_{22}y + h_{23}}{h_{31}x + h_{32}y + h_{33}} \tag{20}$$

Through manual selection or automated feature matching, corresponding pixels (x, y) and (u, v) can be found between two image planes. Therefore, from one corresponding pixel point, 2 equations can be formed. As there are 8 unknown parameters in the homography matrix, we need more than

TABLE I: Notations used in the projective transformation

Notation	Meaning
X_w, Y_w, Z_w	World coordinates
X_c, Y_c, Z_c	Camera coordinate system
$R_{3\times3}$	3×3 rotation matrix converting world to camera coordinates
$T_{3\times1}$	3×1 translation matrix moving world to camera coordinates
x_0, y_0	The intersection point of optic axis and the image plane
a	Aspect ratio
s	Skew of the image plane
λ	Focal length of camera
u, v	Projection of X_w, Y_w, Z_w image plane

Authorized licensed use limited to: Concordia University Library. Downloaded on July 20,2021 at 14:25:49 UTC from IEEE Xplore. Restrictions apply.

4 correspondences (3 of them non-collinear) to estimate the homography matrix. Rearranging (19) and (20), it can be formulated as such:

$$\begin{bmatrix} -x_1 & -y_1 & 1 & 0 & 0 & 0 & x_1u_1 & y_1u_1 & u_1 \\ 0 & 0 & 0 & -x_1 & -y_1 & 1 & x_1v_1 & y_1v_1 & v_1 \\ -x_2 & -y_2 & 1 & 0 & 0 & 0 & x_2u_2 & y_2u_2 & u_2 \\ 0 & 0 & 0 & -x_2 & -y_2 & 1 & x_2v_2 & y_2v_2 & v_2 \\ & & & & \vdots & & & & \end{bmatrix} \begin{bmatrix} h_{11} \\ h_{12} \\ h_{13} \\ h_{21} \\ h_{22} \\ h_{23} \\ h_{31} \\ h_{32} \\ h_{33} \end{bmatrix} = 0 \tag{21}$$

or in other words, $Ah = 0$. This equation can be solved either by calculating the singular value decomposition (SVD) of A or by the eigenvalues of A^TA matrix. In the SVD method, the last column of V matrix is the estimated value of h vector. If the eigenvalue method is used, the h vector is the eigenvector of the lowest eigenvalues.

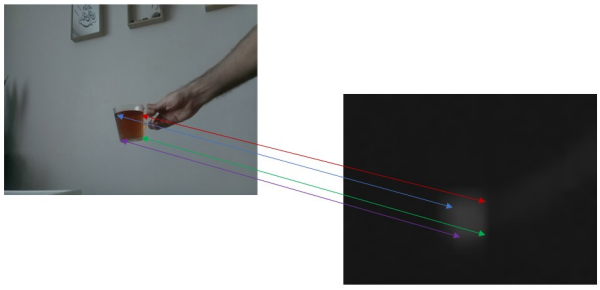

Fig. 8: Aligning corresponding pixels

In this research, the SVD technique is used for estimating the homography matrix. The corresponding points between visual and thermal images are selected manually. The process is illustrated in Fig. 8. Finding the exact correspondent point is challenging because of the different natures between the visual and thermal images. To find the corresponding points, hot red tea in a cup is used because of its visibility in both images with a regular shape. It appears rectangular in both images and the four corners could be somewhat identified. 22 of such images are taken from different distances and angles. These images are used with 4 correspondence points from each pair of images to form A matrix. Two thresholds are imposed onto the visual and thermal images, resulting in a binary image containing potential fire information. Using the computed homography matrix, the thresholded thermal image is aligned and superimposed onto the thresholded visual image. If the suspected fire region from both images are overlapped, it could be concluded that there is a fire in the image.

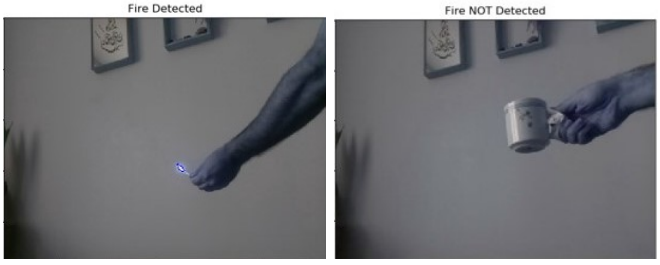

(a) Fire detected in both images (b) Fire not detected in both images

Fig. 9: Fire detection using both camera images

D. Image-Based Thermo-Visual Servoing by the 2DOF Frame

Visual servoing algorithms make use of visual information to control a system. There are two major branches: position-based visual servoing (PBVS) and image-based visual servoing (IBVS). In PBVS, visual information is used to reconstruct the target's pose in a Cartesian space while in IBVS some image features are extracted and used to control the system. In this research, image-based thermo-visual servoing (IBTVS) is used to find the position of a fire and to move the cameras toward the fire. If a fire is detected, the system calculates the relational position of the fire in image coordinate system. This position is sent to the controller and the 2DOF frame will rotate cameras towards the fire.

To create an IBTVS feedback controller for the system that is illustrated in Fig. 3, the first step is to create the error signals represented as follows:

$$\begin{bmatrix} e_x \\ e_y \end{bmatrix} = \begin{bmatrix} x_d - x \\ y_d - y \end{bmatrix} \tag{22}$$

where e_x and e_y are the errors in x and y directions, and x_d and y_d are the desired positions in x and y directions.

The goal is to track the fire location, in other words, to put the fire in the center of the image of camera, i.e. $x_d = y_d = 0$. By imposing the control law of $\dot{e} = Ke$ to (12), a proportional (P) controller is designed as below:

$$\begin{bmatrix} \omega_x \\ \omega_y \end{bmatrix} = \begin{bmatrix} k_1 & 0 \\ 0 & k_2 \end{bmatrix} \times J_{image}^{-1} \begin{bmatrix} e_x \\ e_y \end{bmatrix} = K \times J_{image}^{-1} \begin{bmatrix} e_x \\ e_y \end{bmatrix} \tag{23}$$

K is the proportional gain matrix which tunes the convergence rate of $[x\ y]^T$ towards $[0\ 0]^T$. In experimental tests, this means that the UAV will be navigated towards the fire location. Fig. 10 illustrates the diagram of the IBTVS feedback controller.

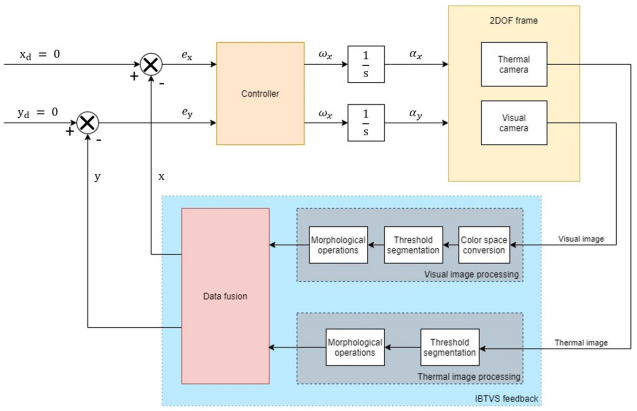

Fig. 10: Diagram of the IBTVS feedback controller

IV. Test Results and Analysis

The experimental results of detection and tracking tests with the 2DOF frame are presented and analysed in this section. The goal of the tests is to validate and demonstrate the capabilities of the developed system with constant detection and tracking of a fire. This way, by knowing the angles, the location of the fire can be found. If a fire is detected, a fire signal can be sent to the base along with its location. In the

Authorized licensed use limited to: Concordia University Library. Downloaded on July 20,2021 at 14:25:49 UTC from IEEE Xplore. Restrictions apply.

tests, a candle representing a fire is used. The system is able to track the flame of the candle and detect its location in terms of angles.

Fig. 11(a) illustrates the angles of camera and the fire. Fig. 11(b) shows the errors of the fire in terms of pixels. Fig. 11(a) is represented in terms of angle (deg) and Fig. 11(b) is represented in terms of pixel because the location of a fire should be expressed in the global coordinate system in order to report to an external observer or a manager who is in charge of fire detection, protection and management in the presence of a forest fire or other fire detection and management applications when a UAV is used for such a mission. While the error should be represented in the camera coordinate system because it is used to generate the control signal in that coordinate system. The experimental test results demonstrate that the developed IBTVS system can detect the fire and guide UAV to track the fire.

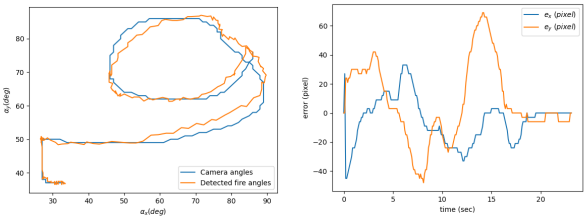

(a) IBTVS tracking test (b) IBTVS tracking errors

Fig. 11: IBTVS test results

V. Conclusion and Future Work

A UAV-based forest fire detection system is developed in this work. The system developed uses one visual and one thermal camera to detect the fire. The images of these two cameras have been fused for effective and reliable detection. To do so, an alignment process has been formed. Next, a 2DOF frame has been fabricated to simulate the UAV and its on-board cameras. Finally, an image-based thermo-visual servoing controller has been designed for detecting and tracking the fire. The real-time experimental test results demonstrate that this system is able to detect, locate and track the fire. Possible future works are 1) conducting field tests to verify the system in real conditions; 2) making use of smoke as another feature of fire to increase the chances of detecting forest fires; 3) calculating the propagation path of the fire as this can help firefighters suppress the fire better and more efficient.

References

[1] J. Martinez-de Dios, B. Arrue, A. Ollero, L. Merino, and F. Gómez-Rodríguez, "Computer vision techniques for forest fire perception," *Image and Vision Computing*, vol. 26, no. 4, pp. 550–562, 2008.

[2] S. Rudz, K. Chetehouna, A. Hafiane, H. Laurent, and O. Séro-Guillaume, "Investigation of a novel image segmentation method dedicated to forest fire applications," *Measurement Science and Technology*, vol. 24, no. 7, p. 075403, 2013.

[3] T. Ingalsbee and U. Raja, "The rising costs of wildfire suppression and the case for ecological fire use," pp. 348–371, Elsevier, 2015.

[4] K. Skala and A. Dubravić, "Integrated system for forest fire early detection and management," *Periodicum Biologorum*, vol. 110, no. 2, pp. 205–211, 2008.

[5] V. G. Ambrosia and T. Zajkowski, *Selection of Appropriate Class UAS/Sensors to Support Fire Monitoring: Experiences in the United States*, pp. 2723–2754. Dordrecht: Springer Netherlands, 2015.

[6] R. S. Allison, J. M. Johnston, G. Craig, and S. Jennings, "Airborne optical and thermal remote sensing for wildfire detection and monitoring," *Sensors*, vol. 16, no. 8, p. 1310, 2016.

[7] E. den Breejen, M. Breuers, F. Cremer, R. Kemp, M. Roos, K. Schutte, and J. De Vries, "Autonomous forest fire detection," *3rd Int. Conf. on Forest Fire Research*, pp. 2003–2012, 1998.

[8] A. E. Çetin, K. Dimitropoulos, and et al., "Video fire detection – Review," *Digital Signal Processing*, vol. 23, no. 6, pp. 1827–1843, 2013.

[9] F. A. Hossain, Y. M. Zhang, and C. Yuan, "A survey on forest fire monitoring using unmanned aerial vehicles," in *2019 3rd International Symposium on Autonomous Systems (ISAS)*, pp. 484–489, 2019.

[10] C. Yuan, Z. X. Liu, and Y. M. Zhang, "UAVs-based forest fire detection and tracking using image processing techniques," in *2015 International Conference on Unmanned Aircraft Systems (ICUAS)*, pp. 639–643, 2015.

[11] T. Celik, H. Ozkaramanlt, and H. Demirel, "Fire pixel classification using fuzzy logic and statistical color model," in *2007 IEEE International Conference on Acoustics, Speech and Signal Processing-ICASSP'07*, vol. 1, pp. 1205–1208, 2007.

[12] T. H. Chen, P. H. Wu, and Y. C. Chiou, "An early fire-detection method based on image processing," in *2004 International Conference on Image Processing*, vol. 3, pp. 1707–1710, 2004.

[13] T. Çelik and H. Demirel, "Fire detection in video sequences using a generic color model," *Fire Safety Journal*, vol. 44, no. 2, pp. 147–158, 2009.

[14] C. Yuan, K. A. Ghamry, Z. X. Liu, and Y. M. Zhang, "Unmanned aerial vehicle based forest fire monitoring and detection using image processing technique," in *2016 IEEE Chinese Guidance, Navigation and Control Conference (CGNCC)*, pp. 1870–1875, 2016.

[15] V. Ambrosia, S. Wegener, D. Sullivan, S. Buechel, S. Dunagan, J. Brass, J. Stoneburner, and S. Schoenung, "Demonstrating UAV-acquired real-time thermal data over fires," *Photogrammetric Engineering Remote Sensing*, vol. 69, pp. 391–402, 2003.

[16] Wonjae Lee, Seonghyun Kim, Yong-Tae Lee, Hyun-Woo Lee, and Min Choi, "Deep neural networks for wild fire detection with unmanned aerial vehicle," in *2017 IEEE International Conference on Consumer Electronics (ICCE)*, pp. 252–253, 2017.

[17] A. E. Ononye, A. Vodacek, and E. Saber, "Automated extraction of fire line parameters from multispectral infrared images," *Remote Sensing of Environment*, vol. 108, no. 2, pp. 179–188, 2007.

[18] L. Merino, F. Caballero, J. R. Martinez-de Dios, and A. Ollero, "Cooperative fire detection using unmanned aerial vehicles," in *Proceedings of the 2005 IEEE International Conference on Robotics and Automation*, pp. 1884–1889, 2005.

[19] J. R. Martínez-de Dios, L. Merino, and A. Ollero, "Fire detection using autonomous aerial vehicles with infrared and visual cameras," *IFAC Proceedings Volumes*, vol. 38, no. 1, pp. 660–665, 2005.

[20] J. Martinez-de Dios and A. Ollero, "A new training-based approach for robust thresholding," in *Proceedings World Automation Congress*, vol. 18, pp. 121–126, 2004.

[21] E. Pastor, A. Àgueda, J. Andrade Cetto, M. Muñoz Messineo, Y. Perez, and E. Planas, "Computing the rate of spread of linear flame fronts by thermal image processing," *Fire Safety Journal*, vol. 41, pp. 569–579, 2006.

[22] C. Yuan, Z. X. Liu, and Y. M. Zhang, "Fire detection using infrared images for UAV-based forest fire surveillance," in *2017 International Conference on Unmanned Aircraft Systems (ICUAS)*, pp. 567–572, 2017.

[23] I. Bosch, A. Serrano, and L. Vergara, "Multisensor network system for wildfire detection using infrared image processing," *The Scientific World Journal*, vol. 2013, p. 402196, 2013.

[24] J. R. Martinez-de Dios, J. André, J. Gonçalves, B. Arrue, A. Ollero, and D. Viegas, "Laboratory fire spread analysis using visual and infrared images," *Int. Journal of Wildland Fire*, vol. 15, pp. 179–186, 2006.

[25] C. Yuan, Z. X. Liu, and Y. M. Zhang, "Vision-based forest fire detection in aerial images for firefighting using UAVs," in *2016 International Conference on Unmanned Aircraft Systems (ICUAS)*, pp. 1200–1205, 2016.

Authorized licensed use limited to: Concordia University Library. Downloaded on July 20,2021 at 14:25:49 UTC from IEEE Xplore. Restrictions apply.